GA–A22471

DIII–D TOKAMAK CONCEPT IMPROVEMENT RESEARCH

by
V.S. CHAN for The DIII–D TEAM

SEPTEMBER 1996

GA–A22471

DIII–D TOKAMAK CONCEPT IMPROVEMENT RESEARCH

by
V.S. CHAN for The DIII–D TEAM

This is a preprint of a paper to be presented at the Sixteenth IAEA International Conference on Plasma Physics and Controlled Nuclear Research, October 7–11, 1996, Montreal, Canada, and to be published in *The Proceedings.*

Work supported by
the U.S. Department of Energy under Contract Nos.
DE-AC03-89ER51114, DE-AC05-96OR22464,
W-7405-ENG-48, DE-A C04-94AL850090, and Grant Nos.
DE-FG03-86ER53266 and DE-FG03-95ER54294

GA PROJECT 3466
SEPTEMBER 1996

DIII–D TEAM

S.L. Allen,[a] P.M. Anderson, M.E. Austin,[b] D. Baggest, F.W. Baity,[c] D.R. Baker, D.E. Baldwin, G. Barber,[c] C.B. Baxi, J.D. Broesch, N.H. Brooks, D. Buchenauer,[d] K.H. Burrell, R.W. Callis, G.L. Campbell, T.N. Carlstrom, E. Carolipio,[e] W.P. Cary, V.S. Chan, M. Chance,[f] E. Chin, H. Chiu, S.C. Chiu, M.S. Chu, S. Coda,[g] J. Cuthbertson,[h] J.C. DeBoo, J.S. deGrassie, G. Diao,[i] J.L. Doane, E.J. Doyle,[j] T.E. Evans, M.E. Fenstermacher,[a] J.R. Ferron, D.K. Finkenthal,[k] R.K. Fisher, R Fitzpatrick,[l] C.B. Forest, J. Freeman, R.L. Freeman, T. Gianakon,[m] P. Gohil, A.M. Gootgeld, J. Greene, K.L. Greene, C.M. Greenfield, R.J. Groebner, H.J. Grunloh, T.E. Harris, R.W. Harvey, W.W. Heidbrink,[e] P.A. Henline, D.N. Hill,[a] D.L. Hillis,[c] F.L. Hinton, T.R. Hodapp, D.J. Hoffman,[c] J. Hogan,[c] K.L. Holtrop, M.A. Hollerbach, R-M. Hong, W. Houlberg,[c] C.L. Hsieh, D.A. Humphreys, A.W. Hyatt, H. Ikezi, G.L. Jackson, F. Jaeger,[c] G. Jahns,[n] T. Jarboe,[o] T.H. Jensen, T. Jernigan,[c] E. Joffrin,[p] R. Jong,[a] R. Junge, Y. Kawano,[q] K.M. Keith, A.G. Kellman, D.H. Kellman, R. Khayrutdinov,[r] K.W. Kim,[j] Y. Kim, C.C. Klepper,[c] J.A. Konings,[s] R.J. La Haye, L.L. Lao, C.J. Lasnier,[a] G.J. Laughon, E.A. Lazarus,[c] B. Lee,[j] J.-H. Lee,[j] R. Lee, R. Lehmer,[h] A.W. Leonard, J.A. Leuer, Y-R. Lin-Liu, J.M. Lohr, G. Lu, T.C. Luce, S. Luckhardt,[h] V. Lukash,[r] J.L. Luxon, M.A. Mahdavi, R. Maingi,[t] M.E. Mauel,[u] W.B. McHarg, G. McKee,[c] R.L. Miller, P.K. Mioduszewski,[c] C.P. Moeller, G. Monier,[p] R.A. Moyer,[h] M. Murakami,[c] G.A. Navratil,[u] A. Nerem, D. Nilson,[a] R.C. O'Neill, T.H. Osborne, L. Owen,[c] R. Patterson, W.A. Peebles,[j] B. Penaflor, Q. Peng, P.l. Petersen, T.W. Petrie, C.C. Petty, D.A. Phelps, W. Phelps, J. Phillips, R.l. Pinsker, P.A. Politzer, D. Ponce, M. Porkolab,[g] G.D. Porter,[a] R. Prater, A. Reiman,[f] E.E. Reis, D. Remsen, C. Ren,[m] M.E. Rensink,[a] C.L. Rettig,[j] G. Rewoldt,[f] T.L. Rhodes,[j] B.W. Rice,[a] J. Robinson, J. Rogers,[f] M. Rosenbluth,[h] D.A. Rothwell, E. Ruskov,[e] S. Sabbagh,[u] O. Sauter,[v] M.J. Schaffer, D.P. Schissel, J.T. Scoville, D.L. Sevier, T.C. Simonen, A. Sips,[w] J.P. Smith, R.T. Snider, F. Söldner,[w] G.M. Staebler, B.W. Stallard,[a] R.D. Stambaugh, H. St. John, R.E. Stockdale, E.J. Strait, D.W. Swain,[c] P.L. Taylor, T.S. Taylor, T. Terpstra,[f] D.M. Thomas, J.F. Tooker, A.D. Turnbull, F. Waelbroeck,[l] M.L. Walker, M.R. Wade,[c] R.E. Waltz, J.G. Watkins,[d] W.P. West, D.G. Whyte,[x] D. Wròblewski,[n] C.P.C. Wong, R.D. Wood,[a] X. Wu,[y] D. Zhang,[y] and J. Zhang[h]

PERMANENT ADDRESS

(*a*) Lawrence Livermore Natl Lab., USA
(b) U. of Maryland, USA
(c) Oak Ridge Natl Lab., USA
(d) Sandia Natl Labs, USA
(e) U. of California at Irvine, USA
(f) Princeton Plasma Phys. Lab., USA
(g) Massachusetts Institute of Technology, USA
(h) U. of California at San Diego, USA
(i) Southwestern Institute of Phys., China
(j) U. of California at Los Angeles, USA
(k) U. of California at Berkeley, USA
(l) U. of Texas at Austin, USA
(m) U. of Wisconsin, USA
(n) ORINCON Corp., USA
(o) U. of Washington, USA
(p) Commissariat a'l'energie Atomique, France
(q) Japan Atomic Energy Research Institute, Japan
(r) TRINITI, Russia
(s) FOM Inst., The Netherlands
(t) Oak Ridge National Universities, USA
(u) Columbia U., USA
(v) EPFL, Switzerland
(w) JET, United Kingdom
(x) INRS — Energie et Materiaux, Canada
(y) ASIPP, China

F1–CN-64/O1–6

ABSTRACT

DIII–D TOKAMAK CONCEPT IMPROVEMENT RESEARCH.

Recent results in tokamak performance optimization and understanding through shape and plasma profile control have brought DIII–D closer to its goal of advanced tokamak (AT) demonstration ($H \equiv \tau_E/\tau_{ITER89P}$ up to 4, and $\beta_N \equiv \beta_T/(I/aB)$ up to 6, simultaneously in steady-state). A high performance regime characterized by negative central magnetic shear (NCS) has resulted in a high β_N *H product of up to 18, and $Q_{dt\text{-}equivalent} = 0.32$. Strong plasma shaping coupled with the control of current and pressure profiles are responsible for the improvement in magnetohydrodynamic (MHD) stability, and stabilization of microturbulence by sheared ExB flow plays a dominant role in the reduction of transport. Density control and helium exhaust are demonstrated with divertor pumping, and reduction of heat flow to the divertor by an order of magnitude through radiative cooling suggests an effective heat exhaust scheme compatible with AT operation. Active current profile control using a combination of neutral beam, bootstrap current and fast wave has been initiated. Achievement of long-pulse AT operation is the future focus of the DIII–D Program.

1. INTRODUCTION

The objective of tokamak concept improvement research is to identify a cost effective and shorter time scale path for the development of the tokamak as a fusion power plant. For a more economical and environmentally attractive fusion power plant, the requirements are: high fusion power density (high β), high ignition margin (high τ_E), continuous operation with low recirculating power (high bootstrap fraction) and adequate heat removal and impurity and particle control. The developmental path can be significantly shortened if improvements in the four areas can be separately or simultaneously demonstrated in existing tokamak facilities, concomitant with development of good scientific understanding and predictive capability. The DIII–D tokamak (Fig. 1) with its unique flexibility to assess a wide range of configurations and operating regimes is well suited for exploring AT operation through active control of the plasma shape and plasma profiles. It also has available a 20 MW neutral beam (NB) system, a 6 MW fast wave (FW) system and a 1 MW electron cyclotron heating (ECH) system (up to 3 MW of ECH in the near future) for extending the duration of the high performance regimes to demonstrate steady-state relevance. Its divertor provides the pumping capability for particle control and heat exhaust. Additionally, a comprehensive set of spatially and temporally resolved diagnostics provides detailed measurements essential for developing the scientific understanding.

In this paper, we report progress in the past two years on the optimization and understanding of these four key areas of research in the DIII–D tokamak and the effort in integrating the progress into a self-consistent advanced tokamak scenario relevant to a fusion power plant.

2. ADVANCED TOKAMAK OPERATION IN DIII–D

Recently a high performance mode involving a negative central magnetic shear (NCS) configuration in DIII–D has demonstrated attractive stability, confinement and bootstrap alignment properties which are desirable for a compact ignition machine. The NCS regime is a modification of the internal magnetic structure which is theoretically predicted to improve performance. Both a reduction and an increase in magnetic shear from that obtained in a standard ohmically driven discharge are predicted to be favorable [1], and this leads to the development of two AT operational regimes: NCS and high internal inductance (ℓ_i). For the past two years, DIII–D has concentrated mostly on the NCS path to high performance.

NCS discharges are characterized by a non-monotonic safety factor (q) profile and the existence of internal transport barriers supporting steep gradients in T_i, T_e, n_e, V_ϕ, as shown in Fig. 2. L–mode and H–mode NCS discharges with inside limiter, single-null divertor (SND), and double-null divertor (DND) configurations have been

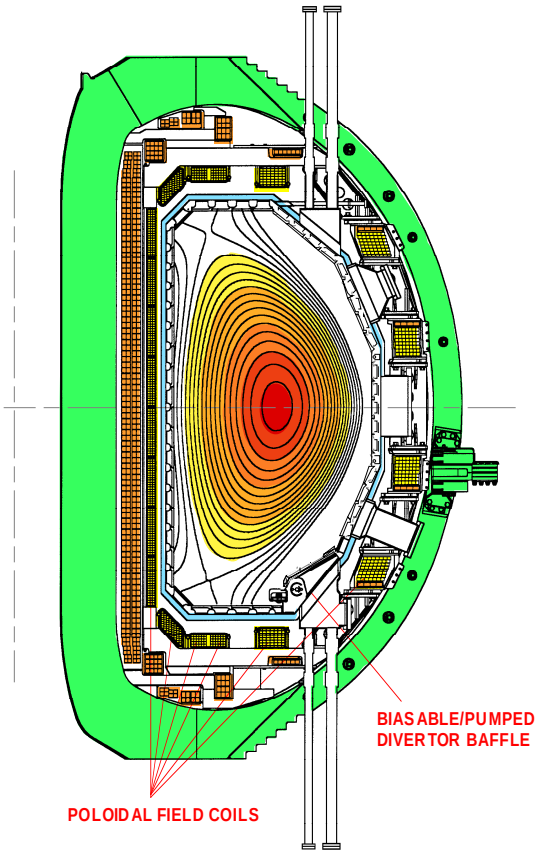

Fig. 1. Cross section of the DIII–D tokamak: 18 individually controlled poloidal field coils and the existing pumped divertor are indicated.

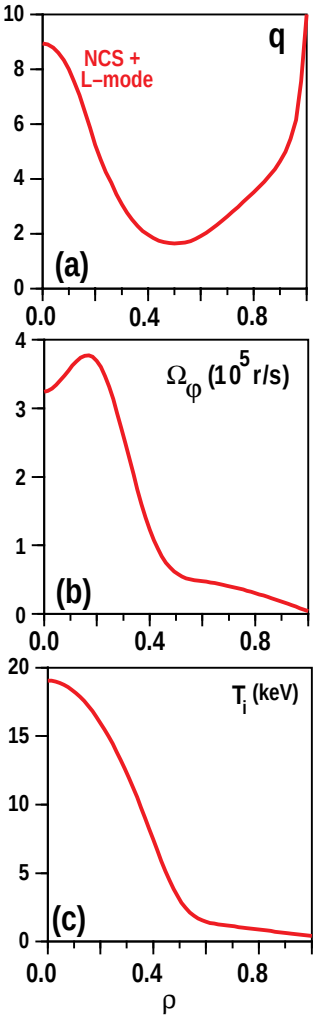

Fig. 2. Characteristic features of NCS discharges: non-monotonic (a) q-profile, internal transport barriers in (b) T_i and (c) Ω_ϕ.

produced in DIII–D. Figure 3 summarizes the highest performance NCS discharge [2] which is a high triangularity DND configuration; achieved parameters are $\beta_N = 4.0$ $\beta_T = 6.7\%$ at $B_T = 2.1$ T, H $\gtrsim$ 4.0,W = 4.2 MJ and $\tau_E = 0.4$s. This discharge reached a new DIII–D record in fusion neutron yield of $Q_{DD} = 1.5 \times 10^{-3}$, corresponding to $Q_{DT}^{eq} = 0.32$. Compared with the previous highest Q_{DD} discharge (which is a hot ion VH–mode), the increase in neutron yield can be attributed to a larger volume of enhanced confinement.

2.1. High Beta Regimes

The NCS approach aims to access the second stable regime to ballooning mode in the plasma core using current profile control. The first NCS discharge on DIII–D was produced by rapid shape elongation with high power NB heating [3]. β_T (0) of 44%was achieved demonstrating access to a second stable core. More recent NCS discharges are produced using NB injection into a low density target plasma during the early current ramp-up phase (Fig. 4). The beam heating raises the plasma temperature rapidly which lengthens the current diffusion time. As a result, the hollow current profile even though not in steady-state remains hollow for a longer duration [4]. This allows study of stability and transport properties in the absence of a steady-state profile control tool. Early beam injection in concert with rapid current ramp-up has become the method of choice for many tokamaks including DIII–D, JET, JT60-U, Tore Supra, and TFTR [5] to produce and study negative magnetic shear configurations.

In DIII–D, NCS plasma core can exist in combination with different edge conditions including L–, H– and VH–mode with different pressure profiles. The β limit due to kink modes critically depends on the plasma shape and pressure profile. The highest β_N achieved ($\beta_N \sim 5$) is in a high triangularity (δ) NCS H–mode with a relatively broad pressure profile [6]. The higher β_N limit with strong shaping is qualitatively consistent with ideal MHD theory. However, theoretical studies using optimized profiles predict further improvement in β_N may be possible [7]. The high β phase is sustained for only a short duration and is terminated by either a soft collapse or a slow decay to lower β values (Fig. 4). The soft collapse, which results in a drop in β but does not terminate

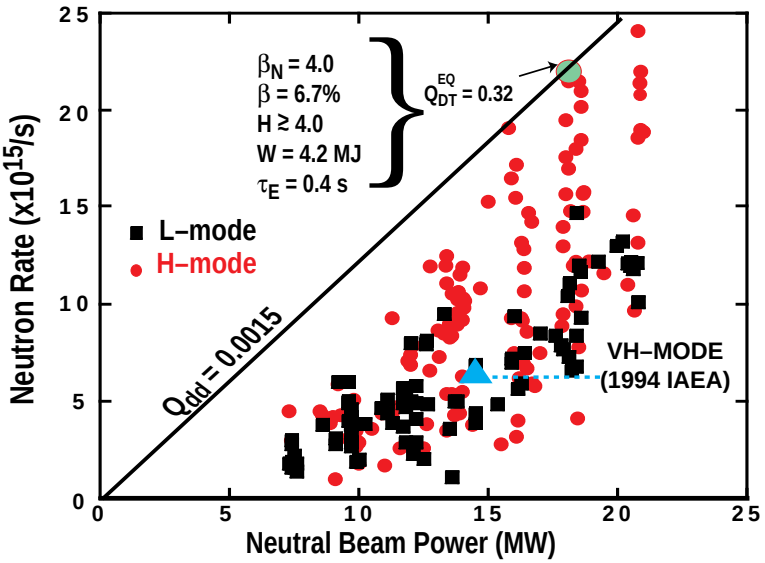

Fig. 3. Fusion performance of NCS discharges in DIII–D

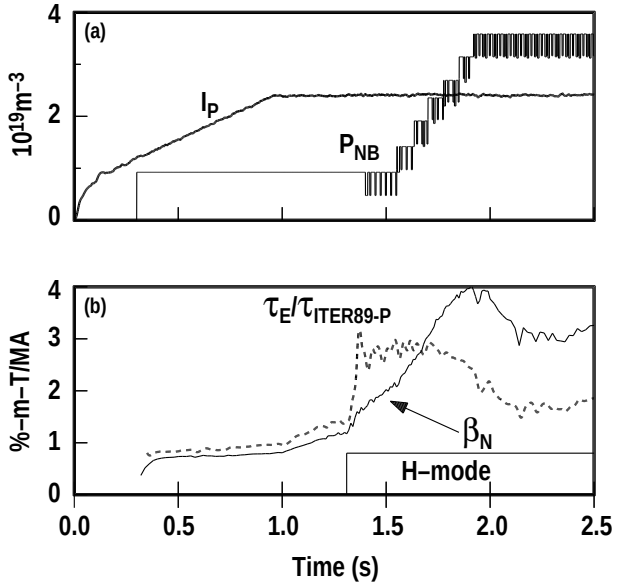

Fig. 4. Time traces showing (a) NCS formation by early NBI during I_p-ramp; (b) temporal behavior of β_N and $\tau_E/\tau_{ITER–89P}$.

the discharge, is usually accompanied by enhanced MHD activities with toroidal mode number n = 2 to 5. The edge motional Stark effect (MSE) diagnostic supports the picture that as the plasma evolves to higher β, the edge builds up a significant bootstrap current and pressure gradient. The discharge becomes susceptible to edge kink mode instability, similar to what has been observed for VH–mode [8]. We believe the edge kink modes are responsible for the loss in stored energy during the collapse. We also found evidence that the vessel wall together with plasma rotation is effective in stabilizing the external modes until the edge current and pressure becomes too large at high β [9]. The slow β decay appears well correlated to the slowly decreasing q-profile in the absence of steady-state current profile control and the onset of MHD activities associated with lower order mode rational surfaces. Theory also predicts the edge kink mode to become more global in character with existence of low mode rational surfaces and can eventually cause the discharge to terminate. Stabilization of the external kink mode and sustainment of the optimum q profile and pressure profile are key factors for increasing β_N further and extending the high β phase of the NCS H–mode.

NCS plasmas with an L–mode edge exhibit very different behavior. They are characterized by highly peaked pressure profiles: $p(0)/\langle p\rangle \sim 5$. While these very peaked pressure profiles contribute to enhanced fusion power production, they often lead to discharge termination with a hard disruption when β_N reaches values of 2.0 to 2.5 [10]. The disruption is preceded by a fast growing rotating n = 1 magnetic precursor with a growth time between the resistive and ideal MHD growth time. The β value at which these discharges terminate is below that predicted by ideal n =1 mode theory. The strong core pressure gradient and large negative magnetic shear result in a condition which violates the resistive interchange stability criterion. Analysis shows that these DIII–D discharges are unstable to localized resistive interchange modes [11]. In Fig. 5, the stability limit against the n = 1 resistive interchange mode is shown in terms of $ß_N$ and $p(0)/\langle p\rangle$. Also shown is the localized structure of this mode. Later in time, a double tearing mode is also found to be unstable. While not yet proven, we suspect hat the resistive interchange coupled with the double tearing instability, which has a

global mode structure, is the cause for the hard disruption. The NCS L–mode appears to behave similarly to the enhanced reverse shear (ERS) mode observed in TFTR, although the termination of ERS has been attributed to internal kink modes [12].

A way of combining the favorable feature of enhanced fusion yield in an NCS L–mode with the higher β limit of NCS H–mode was successfully implemented in DIII–D. This is illustrated in Fig. 6. An NCS L–mode is produced initially and its β and core pressure are allowed to increase with further heating up to the point when the β limit is approached. Plasma shape control is then deployed to induce a transition to H–mode. The density profile flattens quickly resulting in a broadened pressure profile which in turn raises the β limit. This technique allows a steeper core pressure profile than standard H–mode and a higher β than NCS L–mode. Since the fusion production rate depends on optimizing both, this path leads to the highest neutron rate on DIII–D to date $\left(Q_{DT}^{eq}=0.32\right)$ [13].

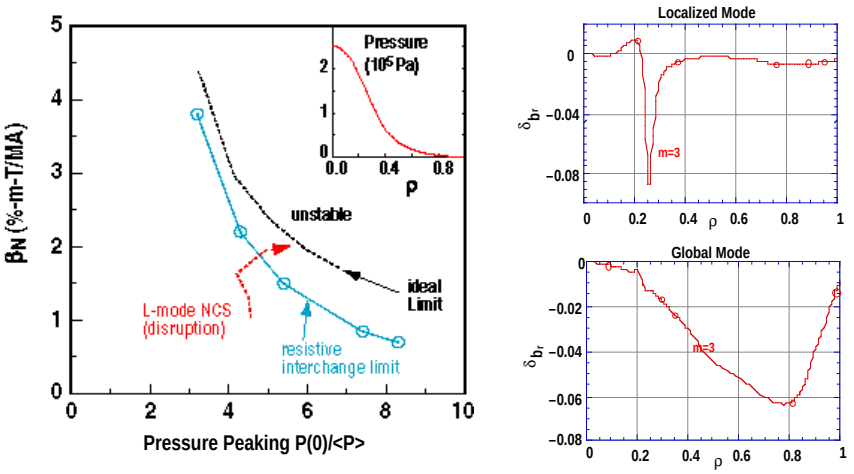

Fig. 5. (a) The b-limits of NCS plasmas vs. pressure profile peakedness p(0)/<p>, (b) Mode structure of resistive interchange mode, (c) mode structure of double tearing mode.

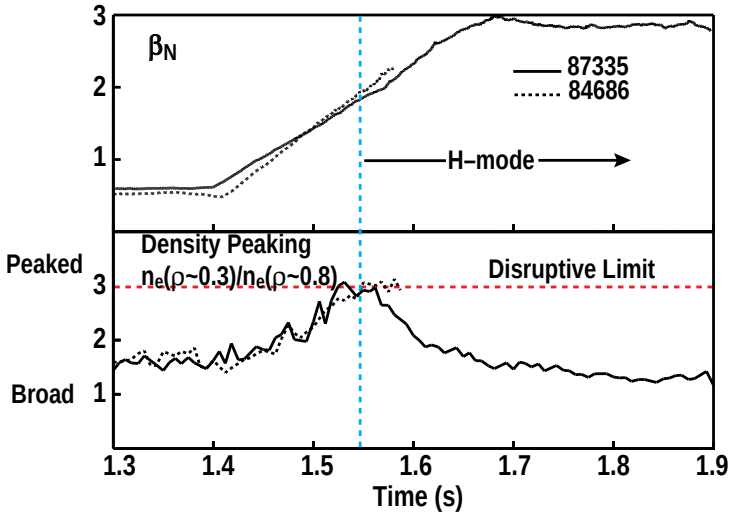

Fig. 6. Evolution of β_N and density profile with transition from L-H mode edge for NCS.

Transitions from L–mode and H–mode is effective in producing a broad pressure profile but does not control the density rise associated with ELM-free H–mode. The density rise reduces core NB heat deposition and current drive efficiency. To gain control of both the density and density profile, an upper divertor pump and baffle is being added to DIII–D for pumping high δ plasma shapes.

2.2. High Confinement Regimes

Transport improvements in plasmas with negative magnetic shear have been seen in many tokamaks: DIII–D, JET, JT60-U, TFTR, and Tore Supra. The improvements are qualitatively similar. Reduction in χ_i and D to neoclassical levels in the plasma core has been observed in DIII–D, JET, JT60-U, and TFTR [5] Significant χ_e reduction has been seen in JT60-U with NBI, and both JT60-U and Tore Supra [14] have observed χ_e reduction using lower hybrid radiofrequency waves for direct electron heating. In DIII–D, when electron heating by FWCD is applied to NCS discharges, reduction in χ_e is also directly observed [15]. Combining NCS with improved edge confinement, DIII–D has successfully demonstrated for the first time transport reduction and turbulence suppression across the entire plasma (Fig. 7). A unifying explanation of the transport improvements in all channels and across the entire plasma is strongly hinted by data from the Charge Exchange Recombination (CER) diagnostic in DIII–D [6,16]. Figure 8 shows strong temporal and spatial correlations between the increase in ExB shear damping calculated using CER data with the transport reduction in regions where the flow shear dominates over microinstability growth rate. This is further supported by physics-based modeling of experiments which includes the effects of ExB shear and magnetic shear stabilization [17]. It is found that the ExB shear damping rate (ω_{ExB}) can become so large as to shut off transport from low-k ion temperature gradient modes (ITG) in all channels allowing only neoclassical transport over a large core plasma. A residual electron heat transport caused by high-k η_e modes may still exist. Their larger growth rates prevent η_e modes from being stabilized by the ExB shear, although the magnitude of their transport is usually quite small. Additionally, Beam Emission Spectroscopy, which measure electrostatic fluctuations in the core, shows local suppression of plasma turbulence. In discharges where the transport is reduced across the entire plasma, far infrared scattering which measures fluctuations across the entire plasma, shows a clear suppression of turbulence across the plasma [18]. An in-out asymmetry in the turbulence is sometimes observed consistent with the ExB flow shear explanation of core transport reduction in NCS discharges.

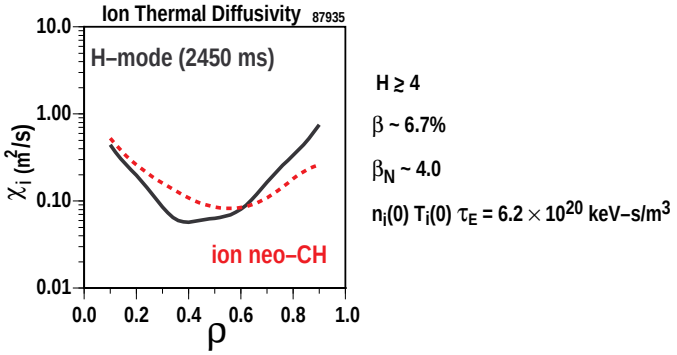

Fig. 7. χ_i is a function of ρ for high performance in NCS H–mode.

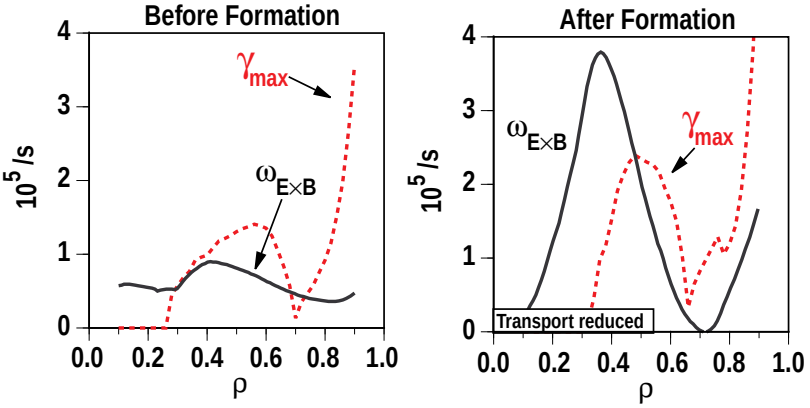

Fig. 8. Comparisonof ExB shearing rate ω_{ExB} and microinstability growth rate γ_{max} before and after transport barrier formation. γ_{max} = ITG growth rate.

What is the role of negative magnetic shear? In DIII–D, we have produced discharges with NCS but no transport improvement. Likewise, TFTR has enhanced reverse shear (ERS) and reverse shear (RS) discharges with the same q-profile but different confinement [12]. Kinetic stability analysis [17,19] of DIII–D discharges confirms that the stabilization effect on the ITG modes by negative magnetic shear alone is not sufficient to explain the core transport barrier formation *i.e.*, the region of improved confinement is broader than the region where ITG modes are stabilized by magnetic shear. There is clearly some correlation between NCS and the internal transport barrier. When it forms, the foot of the transport barrier is at or slightly outside the minimum in safety factor q_{min}. Comparing NCS with hot ion mode, the internal density transport barrier appears to form more readily. When counter-FWCD is used to enhance the NCS, internal transport barrier was more readily established [15]. Analysis has confirmed the NCS region to be in the second stable regime to ballooning modes. This together with $q_{min} > 2$ would allow the core to be free of MHD activities and the development of a much steeper pressure gradient. The high central q value also contributes to enhancing the ExB shear suppression rate. The conclusion we can draw from all the evidence is that magnetic and ExB shear work together in enhancing confinement in NCS plasmas. Magnetic shear and Shafranov shift (local shear) act to lower the growth rate while ExB shear suppresses the residual microturbulence.

Understanding what determines the input power threshold for transport barrier formation is important for projection to future tokamaks. Theory has suggested that the threshold is given by the balance between the microinstability growth rate and the ExB shear damping rate, and the internal transport barrier should first form in the plasma core where the magnetic shear stabilization has the biggest impact [20]. This is corroborated by DIII D measurements which show the core transport barrier first formed in the interior and expanded with increased beam power and contracted with decreased power [18]. The threshold power varies over a wide range in present experiments. DIII–D requires only a few MW to produce the transition to high confinement with internal transport barriers while other tokamaks such as TFTR and JT60-U typically require much higher power. This could perhaps be explained by two possible reasons. The first may be related to the different mechanisms which drive the ExB shear flow. The ExB shear damping rate in toroidal geometry is given by

$$\omega_{ExB} = \left(B_\theta R/B\right) d\left(E_r/RB_\theta\right)/dr \ , \qquad 1/\left(RB_\theta\right) d/dr = d/d\psi \ , \tag{1}$$

and assuming neoclassical ion poloidal velocity,

$$E_r/\left(RB_\theta\right) \cong V_\phi/R + \left(1-K_1\right)/\left(Z_i e\right) dT_i/d\psi + T_i/\left(Z_i e n_i\right) dn_i/d\psi \ , \qquad (2)$$

Since $K_1 \sim 1$ in the plasma core, only toroidal flow and density gradient contribute significantly to producing the ExB flow. DIII–D with tangential NBI can induce turbulence suppression effectively with toroidal flow shear from the toroidal momentum input. This is absent for balanced beam injection in which case the flow is purely diagmagnetic and the flow drive depends largely on the density gradient. High beam power may thus be required to provide a steep density gradient to drive the flow. The second speculation is that the turbulence growth rate and thus the threshold depends strongly on shape in addition to magnetic shear. This is supported by the H–mode power threshold observed in the DIII–D elongation-ramp experiment [21] and is also consistent with a recent experiment to study bean and peapod configurations on DIII–D. Preliminary results from this experiment indicate that these configurations produce transitions to higher confinement modes readily at low input power. The power threshold to enter an enhanced confinement regime is clearly a subject which needs further study if these enhanced confinement modes are to be applied to next step experiments.

3. ISSUES FACING ACCEPTANCE OF AT MODES FOR FUSION POWER PLANTS

3.1. Long Pulse and Steady-State Operation

For an economically attractive fusion power plant, steady-state operation with minimized recirculating power is desirable. This requires operation with high bootstrap current fraction. Combining this with the requirement for high power density, we are led to explore AT modes with both high β_T and β_P. The quantities β_T and β_P are related by

$$\beta_T * \beta_p = 25\left[\left(1+\kappa^2\right)/2\right]\left(\beta_N/100\right)^2 \ , \qquad (3)$$

Simultaneous high β_T and β_P can only be achieved with high β_N and strongly shaped plasmas. DIII–D has produced a variety of discharges including high ℓ_i, high β_P, and NCS modes, with both large β_N and β_P. The high performance phase of all DIII–D discharges with β_N values significantly above 3 lasted only for short durations. The termination of the high β_N phase can be either a soft β collapse (or slow decay) with the plasma settling back to a more modest β_N value, or a hard disruption. To extend the duration of the high performance phase, we have chosen a strategy to avoid the modes with hard disruptions and focus on circumventing the soft β collapses. There is strong evidence that the edge kink mode is a key factor in the β collapse for all high performance discharges with H–mode edge. We believe the steep edge current density and pressure gradient developed with the increased β, the presence of low q rational surfaces and possibly the slowing down of plasma rotation due to loss of beam ions all play a role in destabilizing the edge kink mode. Some progress has been made to develop techniques to control these quantities, although no reliable technique exists for mitigating the edge kink mode and extending the high performance phase duration.

We have explored controlling the edge plasma density of AT modes using the divertor cryopump as a means to control the edge pressure gradient. The cryopump has been shown to be effective in controlling the density and recyling rate for ELMing H–mode plasmas. However, because of its present location, it is only effective for pumping low triangularity (δ), SND plasmas. Since our highest performance NCS H–mode plasmas are high δ DND, ELM-free H–mode plasmas, the present cryopump is not ideal for this purpose. We were encouraged by recent success in producing high performance NCS discharges on DIII–D in JET-shaped plasmas (SND with δ ~ 0.3) with simultaneously achieved values of β_N ~ 4 and H ~ 4. Low amplitude, high frequency ELMs in SND NCS discharges at lower beam power and the cryopump were effectively used to control the edge density and the edge pressure gradient. Key results are depicted in Fig. 9. Approximately constant line-averaged density and values of β_N ~ 3 and H ~ 2.5 were maintained simultaneously for 1.5 s. The β_N * H product is among the highest achieved for H–mode lasting over several τ_E. During this duration, no significant MHD activities were observed indicating some beneficial effect from the edge control. Higher β_N has not been attained because additional power tends to lead to large amplitude ELMs which results in further confinement degradation. The lower δ also lowers the ideal β limit significantly. Since it is easier to produce small amplitude, high frequency ELMs in high δ DND plasmas which also have higher stability limits; an upper pump and baffle for high δ operation, presently being installed, should ease both limitations.

DIII–D has produced a large number of long pulse discharges including H–mode and high β_P mode and with various shapes including ITER-demonstration discharges. These plasmas are maintained by a combination of NB, bootstrap, and radiofrequency driven currents. Some of them have up to 80% bootstrap fraction. They typically have monotonic q-profiles and are limited to β_N < 3 and H < 2. Analysis confirmed that these plasmas are below the ideal β limit. However, attempts to increase β by increasing beam power have resulted in enhanced MHD activities which limit the stored energy and sometimes result in hard disruptions. There is strong indication that this limitation is due to the destabilization of resistive tearing modes by neoclassical bootstrap current [22]. The conditions favoring this are presence of seed islands (possibly introduced by sawteeth and ELMs), positive magnetic shear and low ExB flow. A scaling of the experimentally obtained critical β with collisionality appears consistent

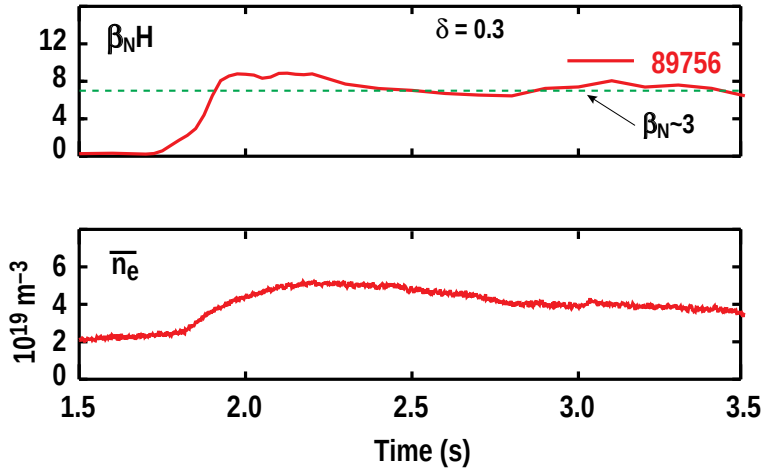

Fig. 9. Long-pulse high performance NCS with ELMing H–mode edge.

with this theory [23]. Because of this result, one might question: even if we can mitigate the edge kink mode for NCS H–mode, will the maximum β be limited by neoclassical tearing mode for long durations? With NCS, absense of sawtooth ($q > 1$) and strong ExB flow, theory would predict stability for NCS discharges. Whether this holds true experimentally can only be answered when we have the off-axis ECRF current drive tool to control the current density profile for long durations.

3.2 Particle Control and Heat Exhaust

We are working to develop methods of particle and heat exhaust compatible with AT operation in the plasma core. In the "standard model" of divertor physics (*i.e.*, classical parallel heat conduction, constant pressure along the field lines, coronal equilibrium radiation rates, and constant impurity concentration in the core, scrape-off-layer (SOL), and divertor) the amount of power that can be radiated in the divertor is directly linked to the core Z_{eff} and dilution. For example, in ITER for light impurities when the core Z_{eff} limit is reached, the standard model only allows 100 MW radiation in the divertor. The remainder of the power exhaust must be made up by core plasma radiation. While results from TEXTOR are promising on maintaining good core performance with a nearly 100% radiative mantle [24], we are concentrating on ways to increase divertor radiation while maintaining low core impurity levels and gas fueling burdens using physics approaches outside the standard model: plasma detachment, 2-D cross-field heat flow effects, non-coronal radiation enhancements, non-thermal distribution effects, and divertor impurity enrichment [25].

We have employed a new divertor Thomson scattering system in conjunction with radial X-point sweeping to make detailed 2-D documentation of divertor plasma detachment , which lowers the divertor plasma temperature and the heat flux to the divertor plates [26] (Fig. 10). In attached plasmas, irrespective of confinement mode or heating mode, we find the total plasma pressure along the field lines in the SOL is conserved to within a factor of two. With detachment produced by deuterium puffing, the pressure drops more than ten times along the separatrix to the divertor strike point while remaining high further out in the SOL; we refer to this condition as a partially detached divertor. We have also found that the electron temperature in the divertor plasma is reduced into the range 1–3 eV, a range where volume recombination of the plasma should be strong. Modeling with the UEDGE code has successfully matched most key features of our divertor data in a detached plasma and shows that volume recombination is a dominant process [27]. Volume recombination increases the radiation from the divertor by producing the recombination power in the plasma rather than in the divertor plate. We have been able to use partially detached plasmas to produce a long (50 cm), radiating divertor leg with only a 2:1 variation of the emission along the leg, exceeding ITER requirement [26] (Fig.11). The aim of the ITER divertor solution is to reduce the peak heat flux at the divertor plate by spreading the heat flux along the divertor channel, but ITER only requires a 6:1 uniform spreading.Preliminary analysis indicates that the length of the radiating zone in Fig. 11 exceeds substantially the predictions of the standard model, requiring investigation of the role of non-coronal and convective effects. The core plasma confinement in the case of Fig. 11 was progressively reduced to the L–mode level by the high neutral pressures (reaching 1 mTorr) near the core plasma that resulted from the strong gas flow through to the divertor pump and the inadequate divertor baffling in DIII–D. The full installation of the double null, triangular plasma, Radiative Divertor in DIII–D will provide the baffling

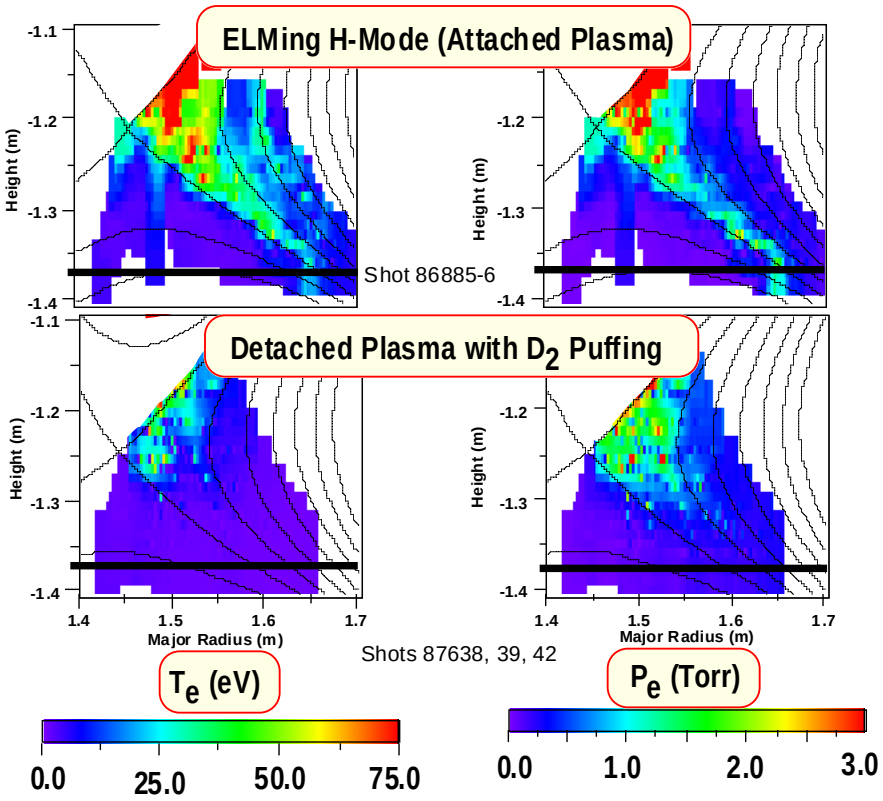

Fig. 10. Divertor Thomson data showing T_e and P_e drop and plasma "detaches" with D_2 pumping.

needed to allow simultaneous high performance core plasmas with low impurity and neutral pressures with high plasma and neutral densities in the detached divertor.

A divertor impurity enrichment (defined as the ratio of impurity concentration in the divertor to the impurity concentration in the core plasma) greater than one can enhance divertor radiation while maintaining limits on core Z_{eff} and radiation. An enrichment of three in ITER would enable essentially all the exhaust power to be radiated in the divertor. Increased enrichment is expected from strong fuel ion flows that drive impurity ions down the field lines overcoming the thermal gradient force that pushes impurity ions up the field lines. In our so-called "puff and pump" experiments in which fuel gas flows up to 150 Tℓ/s are admitted at the top of the machine and exhausted through the divertor pump, we have documented carefully a modest enrichment (1.4–2) [26,28] in the divertor pump plenum using neon impurity gas and obtained preliminary indications of a much larger enrichment using argon impurity gas.

In most divertor tokamaks, attempts to raise the core plasma density above the Greenwald limit have been frustrated by detachment of the divertor leading (under high gas puffing) to a divertor MARFE which migrates into the core plasma. By lightly pumping the divertor and using pellet fueling instead of gas fueling, we have been able to prevent the collapse of the divertor and so gain a view of the physical processes in the plasma core that limit the density. We have obtained densities 1.5 times the Greenwald density limit while maintaining energy confinement at 1.8 times ITER–89P

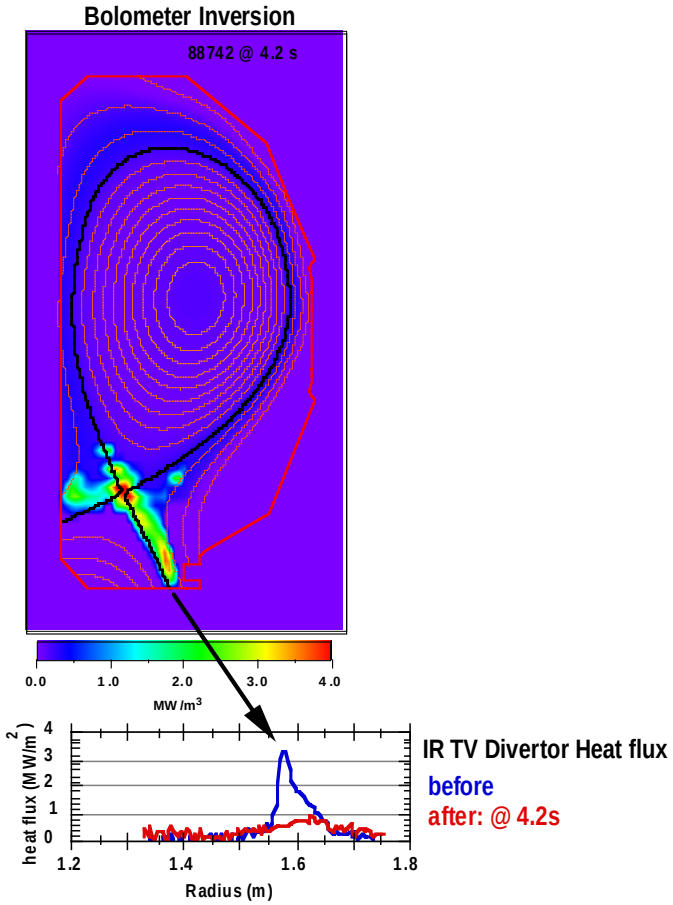

Fig. 11. Long radiating divertor leg demonstrating effective radiation exceeding ITER requirements

scaling [25]. Particle transport after pellets is largely independent of density relative to the Greenwald limit. Core radiative collapses and tearing mode effects are seen.

Our divertor results have provided some strong support of key features of the ITER divertor concept: detached plasmas, radiation distributed uniformly along the divertor leg, and densities above the Greenwald limit. Promising lines of investigation to increase divertor radiation while maintaining clean, high performance core plasmas are being pursued.

3.3. Core Impurity Control in Enhanced Confinement Regimes

Associated with transport reduction is the potential build-up of impurities in the plasma core which will have a deleterious effect on the tokamak performance. For AT operation to be acceptable for fusion power plants, adequate control of impurity contaminants and helium "ash" has to be demonstrated. Experiments have been conducted on DIII–D to characterize both global and local impurity transport characteristics under a variety of conditions. Progress has been made in identifying AT operations in which impurity contamination is simultaneously being minimized.

To address the issue of helium ash exhaust, previous experiments on DIII–D with helium introduced via gas puffing at the plasma edge have shown that sufficient helium exhaust can be achieved $\left(\tau^*_{He}/\tau_E \sim 8\right)$ simultaneously with good energy confinement in an ELMing H–mode plasma [29]. These results have been extended in more recent experiments utilizing helium neutral beam injection as a central source of helium. This central helium source coupled with simultaneous divertor exhaust using a divertor cryopump provide a better simulation of the central source of fusion produced alpha products. In these experiments, substantial helium exhaust is observed with $\tau^*_{He}/\tau_E \sim 8.5$. The measured helium density profile is observed to remain essentially the same during the He beam injection phase after a brief transient. This observation suggests that the exhaust of helium in this case is limited by the effective exhaust efficiency of the pumping configuration and not by helium transport within the plasma core.

In DIII–D, the carbon behavior in NCS discharges appears to be dependent on whether the edge plasma exhibits an L–mode or H–mode character [30]. As illustrated in Fig. 12, for NCS L–mode, both electron and carbon density are observed to increase in the core while the edge carbon density remains nearly constant. Consequently, the carbon concentration and Z_{eff} changes little. In the ELM-free NCS H–mode case, the carbon inventory increases linearly in time during the high confinement phase, accumulating primarily in the plasma edge while the core remains relatively clean. Finally, discharges in which NCS has been maintained simultaneously with ELMs exhibit a clamping and subsequent decrease in carbon concentration once ELMs begin, similar to what is observed in standard ELMing H–mode plasmas.

The DIII–D studies have identified the AT operating conditions most compatible with effective impurity and helium "ash" exhaust as an ELMing H–mode edge with divertor pumping. ELMs are also desirable for self-regulating the edge pressure gradient which is useful for mitigating the edge kink mode instability. At present, the highest performance AT modes are ELM-free discharges. A key focus for the DIII–D AT Program in the future will be to produce enhanced performance NCS H–modes with ELMing edge.

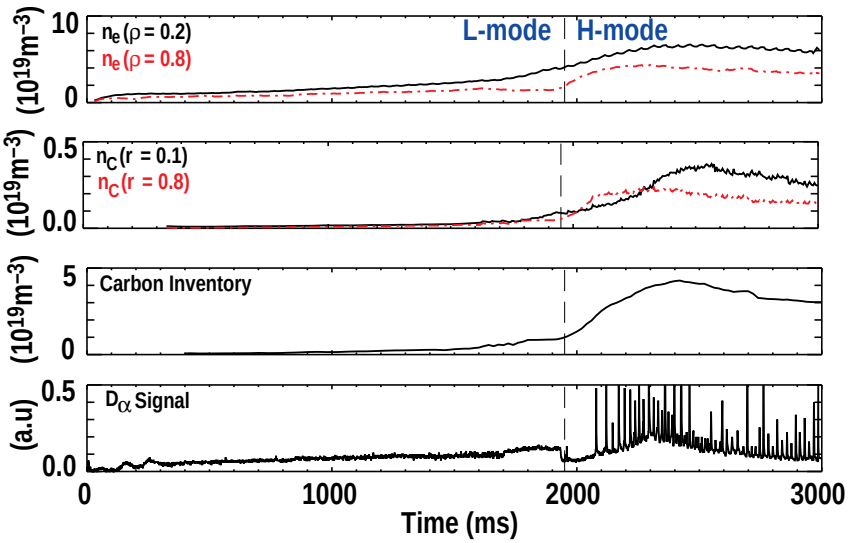

Fig. 12. ELMing NCS H–mode showing a clamping and subsequent decrease in carbon impurities.

4. SUMMARY AND FUTURE DIRECTIONS

A significant achievement in tokamak concept improvement research on DIII–D for the past two years is the development of a reproducible enhanced performance mode which possesses simultaneously attractive stability, transport and bootstrap alignment properties for a compact fusion power plant. This mode is achieved by producing a NCS configuration under several shapes (δ = 0.8 DND and 0.3 SND), and plasma edge conditions (L–, ELM-free H– and ELMing H–mode). The highest performance in terms of fusion gain is achieved for a DND NCS H–mode plasma, achieving a Q_{DD} value of 0.0015. These experiments achieved record stored energy for DIII–D, in excess of 4 MJ, increased the triple product to $n_d(0)Ti(0)\tau_E = 6.2 \times 10^{20}$ keV s m^{-3} , and neutron rates up to 2.2×10^{16} s^{-1}. The highest β_N * H product = 20 with β_N value of 5 and H of 4, is achieved in a weakly negative magnetic shear H–mode plasma. Numerical simulations using optimized pressure profiles indicate further increase in β_N should be achievable. The transport reduction to the neoclassical level and the formation of transport barriers from measurements of core fluctuation and electric field are consistent with theoretical predictions of ExB shear flow suppression of microturbulence.

The high performance phase has only been maintained for relatively short durations (<0.5 s), and is terminated either by a soft β collapse or hard disruption depending on the pressure profile peakedness. MHD instabilities responsible for the termination have been qualitatively identified as edge kink modes and resistive interchange/double tearing modes, respectively. To demonstrate the viability of AT modes for fusion power plants, the existence of steady-state relevant operation has to be proven. To this end, we need to ameliorate the soft β collapse by maintaining the optimized current and pressure profile for enhanced stability and transport. We plan to achieve this by exploring (a) a combination of radiofrequency current drive and well-aligned bootstrap current for current profile control; (b) particle pumping in strongly shaped plasmas for core and edge density control; and (c) the operation of NCS with ELMing H–mode edge.

Electron cyclotron current drive is the key for off-axis current profiles control. With a 3 MW ECH system operational in 1997, we plan to extend the pulse length of NCS discharges significantly. Upgrading the system to 6 MW will allow full demonstration of steady-state operation. We are encouraged by preliminary heating results with the new 110 GHz 1 MW system as shown in Fig. 13. With 0.4 MW out of 1 MW coupled to a low density plasma, T_e of 10 keV has been achieved at $n_e = 5\times10^{18}$ m^{-3}. The DIII–D tokamak is presently being vented to install a new divertor cryopump compatible with high δ AT operation This capability is essential to demonstrate a fully integrated AT scenario. It will be used to explore edge pressure control in DND plasmas including both density and ELM control, divertor detachment and heat exhaust in strongly shaped configuration, and impurity contaminant control in enhanced confinement regimes.

Studies in DIII–D have shown that plasma detachment is effective in reducing the heat flow to the divertor plate. A pressure drop of >10 times with T_e at the plate reduced to 1–3 eV has been achieved. Comparison with numerical modeling has provided insight of dominant atomic physics in low T_e divertor plasma. We will continue to explore the effectiveness of impurity enrichment for radiative divertors. The proposed radiative divertor modification [31] which is now being scheduled for 1998 will allow continuous evolution of the concept and undoubtedly will add to the performance of the divertor.

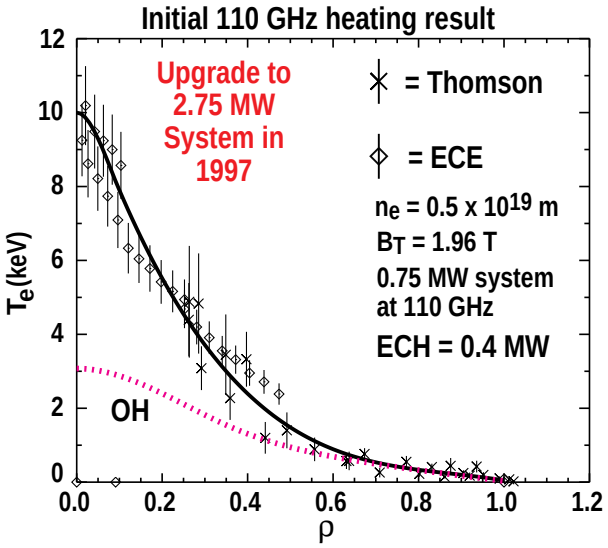

Fig. 13. Te increases with 0.4 MW of electron cyclotron heating at 110 GHz.

In conclusion, the DIII–D tokamak concept improvement research has made significant strides in developing the scientific understanding and predictive capability of AT operating regimes. This underlying understanding accomplished by detailed diagnostic measurements will remain an important element of our research. Looking ahead, the availability of off-axis ECCD and upper divertor pumping will allow the program to proceed with the integrated demonstration of high performance, long-pulse operation compatible with efficient heat exhaust and particle control.

5. REFERENCES

[1] TURNBULL, A.D., et al., Phys. Rev. Lett. **74** 718 (1995); KESSEL, C., et al., ibid, 1212.
[2] LAZARUS, E.A., et al., Phys. Rev. Lett. **77** 2714 (1996); LAZARUS, E.A., et al., "Higher Fusion Power Gain With P:rofile Control in DIII–D Tokamak Plasmas," to be published in Nucl. Fusion.
[3] LAZARUS, E.A., et al., Phys. Fluids **B 4** 3644 (1992).
[4] RICE, B.W.., et al., Plasma Phys. Contr. Fusion **38** 869 (1996).
[5] NAVRATRIL, G.A., et al., "Review of Tokamak Regimes With Negative Magnetic Shear," in Proc. 23rd Euro. Conf. on Contr. Fusion and Plasma Phys., Kiev, Ukraine (European Physical Society, Petit-Lancy, Switzerland) to be published.
[6] LAO, L.L., et al., Phys. Plasmas **3** 1951 (1995).
[7] TURNBULL, A.D., this conference.
[8] STRAIT, E.J., et al., in Proc. 20th Euro. Conf. on Contr. Fusion and Plasma Phys., Lisbon, Portugal (European Physical Society, Petit-Lancy, Switzerland, 1994) Vol. 18B, Part I, p. 211.
[9] STRAIT, E.J.., et al., Phys. Rev. Lett. **74** 2483 (1995).
[10] STRAIT, E.J.., et al., Phys. Rev. Lett. **75** 4421 (1995); RICE, B.W.., et al., Phys. Plasmas **3** 1983 (1995).
[11] CHU, M.S., Phys. Rev. Lett. **77** 2710 (1996).

[12] LEVINGTON, F.M., et al., Phys. Rev. Lett. **75** 4417 (1995).
[13] LAZARUS, E.A., et al., this conference.
[14] USHIGUSA, K., et al., this conference; SAOUTIC, B., et al., this conference.
[15] FOREST, C.R., et al., Phys. Rev. Lett. **77** 3141 (1996); PRATER, R., et al., this conference.
[16] BURRELL, K.H., presentation at Transport Task Force Workshop, Varenna, Italy, 1996; SCHISSEL, D.P., et al., this conference.
[17] WALTZ, R.E.., et al., this conference.
[18] DOYLE, E.J., et al., this conference.
[19] REWOLDT, G., et al., Phys. Plasmas **3** (1996); WALTZ, R.E. Phys. Plasmas **2** 2408 (1995).
[20] STAEBLER, G.M., et al., Phys. Plasmas **1** 909 (1994); DIAMOND. P.H., et al. Phys. Plasmas **2** 3685 (1995).
[21] LAO, L.L., et al., Phys. Rev. Lett. **70** 3435 (1993).
[22] HEGNA, C.C., and CALLEN, J.D., Phys. Plasmas **1** 2308 (1994).
[23] LA HAYE, R.J.., et al., this conference.
[24] WOLF, G.H., et al., this conference.
[25] MAHDAVI, M.A., et al., this conference.
[26] FENSTERMACHER, M.E., "Comprehensive 2-D Measurements of Radiative Divertor Plasmas in DIII–D," in Proc. 12th International Conf. on Plasma Surface Interactions in Contr. Fusion Devices, Saint Raphael, France, to be published in J. Nucl. Mater.
[27] PORTER, G.D., Phys. Plasmas **3** 1967 (1995).
[28] SCHAFFER, M.J., "Direct Measurement of Divertor Exhaust Neon Enrichment in DIII–D," in Proc. 12th International Conf. on Plasma Surface Interactions in Contr. Fusion Devices, Saint Raphael, France, to be published in J. Nucl. Mater.
[29] WADE, M.R., et al., Phys. Rev. Lett. **74** 2702 (1995); WADE, M.R., et al., Phys. Plasmas **2** 2357 (1995).
[30] WADE, M.R., et al., "Characterization Of Core Impurity Transport and Accumulation in Various Operating Regimes in DIII–D," in Proc. 23rd Euro. Conf. on Contr. Fusion and Plasma Phys., Kiev, Ukraine (European Physical Society, Petit-Lancy, Switzerland) to be published.
[31] ALLEN, S.L., et al., Plasma Phys. and Contr. Fusion **37** A191 (1995).